Stiff, and Sticky in the Right Places: The Dramatic Influence of Preorganizing Guest Binding Sites on the Hydrogen Bond-Directed Assembly of Rotaxanes

Francesco G. Gatti,[†] David A. Leigh,*[,†,⊥] Sergey A. Nepogodiev,[†] Alexandra M. Z. Slawin,[§] Simon J. Teat,[‡] and Jenny K. Y. Wong[†]

Contribution from the Centre for Supramolecular and Macromolecular Chemistry, Department of Chemistry, University of Warwick, Coventry CV4 7AL, United Kingdom, Department of Chemistry, University of St. Andrews, Fife KY16 9AJ, United Kingdom, and CLRC Daresbury Laboratory, Warrington, United Kingdom

Received May 16, 2000

Abstract: Structural rigidity and the preorganization of thread binding sites are shown to have a major influence on template efficiency in the synthesis of hydrogen bond-assembled rotaxanes. Preorganization is so effective, in fact, that with good hydrogen bond acceptors (amides) a "world record" yield of 97% for a [2]rotaxane is obtained. The truly remarkable feature of this efficient template, however, is that it allows even poor hydrogen bond acceptors (esters) to be used to prepare hydrogen bond-assembled rotaxanes, despite the presence of competing hydrogen bonding groups (anions) which bind the key intermediates at least 10000× more strongly than single, unorganized, ester groups! The structures of the rotaxanes are established unambiguously in solution by ^{1}H NMR spectroscopy and in the solid state by X-ray crystallography. As a series they provide unique experimental information regarding the nature of amide−ester hydrogen bonding interactions; in particular they suggest that in $CDCl_3$, amide−ester NH···O═C hydrogen bonds are ∼1 kcal mol^{-1} weaker than the corresponding amide−amide interactions.

Introduction

The importance of the preorganization of binding sites in host−guest complexation processes has long been recognized.[1] For example, the structurally rigid spherand **1** binds Li^+ >10^{12} times stronger than the acyclic podand **2** despite near-identical aryl ether−metal ion electrostatic interactions being present in each complex.[2] While the drastically decreased binding of **2** can in part be attributed to the differences in solvation of the free ligands, a significant entropic cost has to be paid to organize the convergent binding sites of the flexible free host into the conformation involved in metal ion complexation. Here we describe how the preorganization of the divergent binding sites of a thread, the "guest"(!), provides a dramatic increase in macrocycle template efficiency, enabling the use of even modest hydrogen bond acceptor groups (esters) in the multicomponent synthesis of hydrogen bond-assembled rotaxanes.[3]

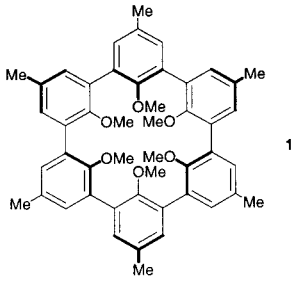

Isophthalamide (benzene 1,3-dicarboxyamide) and peptide-based threads have been shown[4] to template the formation of benzylic amide macrocycles about them in nonpolar solvents to give rotaxanes and molecular shuttles in good (typically 28−62%) yields. The five component "clipping" reactions (Scheme

* Address correspondence to this author. E-mail: David.Leigh@Warwick.ac.uk.
† University of Warwick.
§ University of St Andrews.
‡ CLRC Daresbury Laboratory.
⊥ Address from October 2001: Forbes Chair of Organic Chemistry, Department of Chemistry, University of Edinburgh, The King's Buildings, West Mains Road, Edinburgh EH9 3JJ, United Kingdom.

(1) See, for example: (a) Cram, D. J. *Angew. Chem., Int. Ed. Engl.* **1988**, *27*, 1009−1020. (b) Gerbeleu, N. V.; Arion, V. B.; Burgess, J. *Template Synthesis of Macrocyclic Compounds*; Wiley-VCH: Weinheim, 1999. (c) *Templated Organic Synthesis*; Diederich, F., Stang, P. J., Eds.: Wiley-VCH: Weinheim, 2000.

(2) (a) Cram, D. J.; Lein, G. M. *J. Am. Chem. Soc.* **1985**, *107*, 3657−3668. (b) Cram, D. J.; deGrandpre, M. P.; Knobler, C. B.; Trueblood, K. N. *J. Am. Chem. Soc.* **1984**, *106*, 3286−3292.

(3) For reviews on rotaxanes see, for example: (a) Amabilino, D. B.; Stoddart, J. F. *Chem. Rev.* **1995**, *95*, 2725−2828. (b) *Molecular Catenanes, Rotaxanes and Knots*; Sauvage, J.-P., Dietrich-Buchecker, C., Eds.; Wiley-VCH: Weinheim, 1999.

10.1021/ja001697r CCC: $20.00
Published on Web 06/02/2001

Scheme 1. Rotaxane Formation via Flexible, Peptide-Based Hydrogen Bond Templates (R, R′ = H, Me)

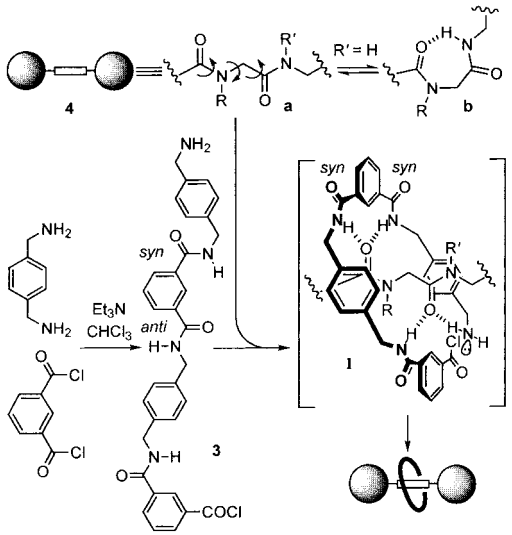

1) are able to produce rotaxanes because the immediate precursor to macrocycle formation, **3**, preferentially adopts a linear conformation as a consequence of the preference for the aromatic 1,3-diamide unit to adopt a syn-anti conformation,[5] which holds the two reactive ends of **3** far apart in a spatial arrangement unsuitable for macrocyclic ring closure. Thus, in the absence of a suitable template, structures such as **3** are long-lived in solution and may even dimerize to form larger macrocycles in preference to intramolecular ring closure.[5a] Under the rotaxane-forming reaction conditions, however, cooperative multipoint hydrogen bonding between the precursor and a thread (e.g. **4**) promotes a conformational change in **3** (the syn-syn rotamer is stabilized by the bifurcated hydrogen bonding motif shown in **I**, Scheme 1) which brings the amine and acid chloride in close proximity leading to rapid cyclization of **3**.[4b] Additional hydrogen bonding interactions between **3** and a *second* site on the thread are important for efficient rotaxane formation since they hold one or both ends of the precusor in appropriate positions, such that the cyclization of **3** occurs *around* the thread to give the mechanically interlocked product.

Although the dipeptide motif is clearly a good template for the benzylic amide macrocycle system, the free thread possesses several internal degrees of freedom that are lost in the key supramolecular complex **I**, including torsional freedom around the three backbone bonds shown in **4a** (Scheme 1). Furthermore, the flexibility of the peptide backbone means that it can adopt additional conformations (e.g. **4b**) reminiscent of γ-turns. These are stabilized by the formation of seven-membered-ring intramolecular hydrogen bonds which, although relatively uncommon in proteins, may be significant in the nonpolar solvents used for promoting rotaxane formation.[6] It seemed likely, therefore, that the unfavorable requirements of breaking intramolecular hydrogen bonds and/or the loss of entropy in going from a flexible thread to the much stricter conformational and co-conformational requirements of the supramolecular transition state could be overcome more efficiently by preorganizing the hydrogen bonding sites of the thread in a spatial arrangement already suited for templating benzylic amide macrocycle formation.

Scheme 2. Rotaxane Formation via Preorganized, Rigid Fumaryl-Based Hydrogen Bond Templates

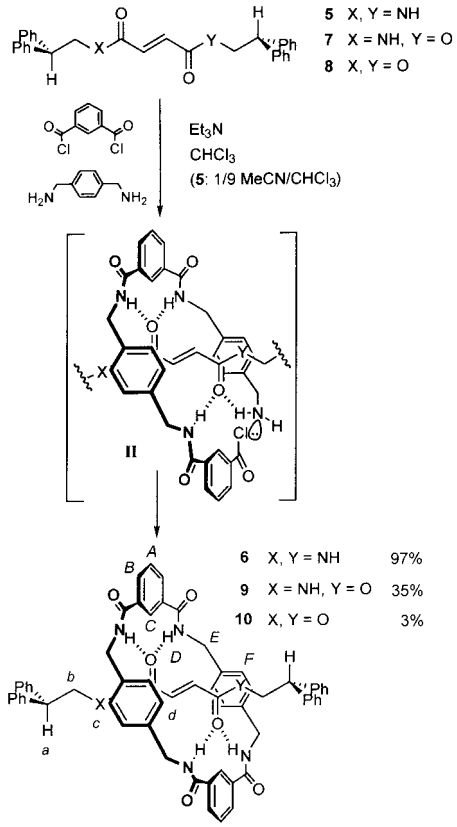

Results and Discussion

The rigid fumaramide thread, **5**, was prepared in one step from the commercially available amine and bis-acid chloride. Treatment of **5** with 4 equiv of xylylene diamine and isophthaloyl dichloride (1:9 MeCN:$CHCl_3$, Et_3N, 4 h, high dilution) was sufficient for complete consumption of the thread. Filtration followed by spontaneous crystallization upon addition of water to a dimethylformamide solution of the crude product led to the rotaxane **6** in 97% yield (Scheme 2). The yield is all the more remarkable considering that fumaramide rotaxanes previously prepared by the Vögtle group are formed in much more modest (18−26%) yields,[7] despite being carried out using a presynthesized macrocycle in a three-component "threading" procedure (which can *only* produce free thread or rotaxane) rather than the intrinsically more demanding five-component clipping method (which, in addition to rotaxane, can produce catenanes, simple macrocycles, linear and higher cyclic oligomers, and polymers). The facile synthesis from commerically available reagents, chromatography-free isolation procedure, and

(4) (a) Johnston, A. G.; Leigh, D. A.; Murphy, A.; Smart, J. P.; Deegan, M. D. *J. Am. Chem. Soc.* **1996**, *118*, 10662−10663. (b) Leigh, D. A.; Murphy, A.; Smart, J. P.; Slawin, A. M. Z. *Angew. Chem., Int. Ed. Engl.* **1997**, *36*, 728−732. (c) Lane, A. S.; Leigh, D. A.; Murphy, A. *J. Am. Chem. Soc.* **1997**, *119*, 11092−11093. (d) Clegg, W.; Gimenez-Saiz, C.; Leigh, D. A.; Murphy, A.; Slawin, A. M. Z.; Teat, S. J. *J. Am. Chem. Soc.* **1999**, *121*, 4124−4129. (e) Leigh, D. A.; Troisi, A.; Zerbetto, F. *Angew. Chem., Int. Ed.* **2000**, *39*, 350−353. (f) Brouwer, A. M.; Frochot, C.; Gatti, F. G.; Leigh, D. A.; Mottier, L.; Paolucci, F.; Roffia, S.; Wurpel, G. W. H. *Science* **2001**, *291*, 2124−2128.

(5) (a) Carver, F. J.; Hunter, C. A.; Shannon, R. J. *J. Chem. Soc., Chem. Commun.* **1994**, 1277−1280. (b) Geib, S. G.; Vincent, C.; Fan, E.; Hamilton, A. D. *Angew. Chem., Int. Ed. Engl.* **1993**, *32*, 119−121. (c) Johnston, A. G.; Leigh, D. A.; Nezhat, L.; Smart, J. P.; Deegan, M. D. *Angew. Chem., Int. Ed. Engl.* **1995**, *34*, 1212−1216.

(6) Dado, G. P.; Gellman, S. H. *J. Am. Chem. Soc.* **1993**, *115*, 4228−4245.

(7) (a) Jäger, R.; Baumann, S.; Fischer, M.; Safarowsky, O.; Nieger, M.; Vögtle, F. *Liebigs Ann./Recl.* **1997**, 2269−2273. (b) Parham, A. H.; Windisch, B.; Vögtle, F. *Eur. J. Org. Chem.* **1999**, 1233−1238.

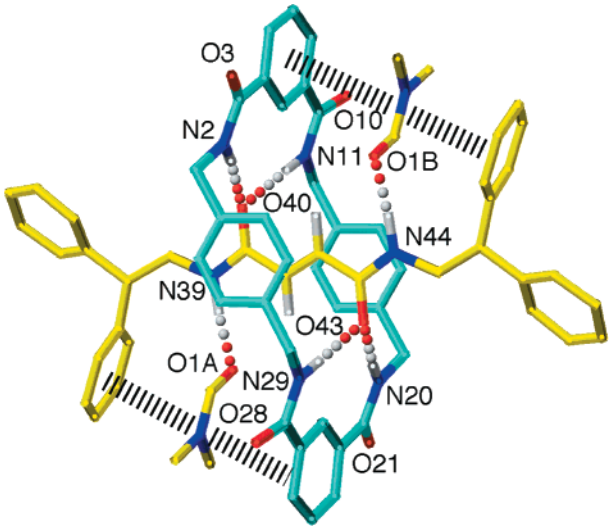

Figure 1. X-ray crystal structure of the fumaramide [2]rotaxane **6** (for clarity carbon atoms of the macrocycle are shown in blue and the carbon atoms of the thread in yellow; oxygen atoms are depicted in red, nitrogen atoms in dark blue, and selected hydrogen atoms in white). Intramolecular hydrogen bond distances (Å) are the following: O40−HN2/O43−HN20 1.98, O40−HN11/O43−HN29 2.06.

"world record" yield for a [2]rotaxane synthesis makes this reaction one of the most effective routes to rotaxane architectures discovered thus far.

Single crystals of **6** suitable for investigation by X-ray crystallography using a synchrotron source were obtained directly from the workup procedure. The crystal structure (Figure 1) shows that the positioning of the amide groups in the fumaramide thread allows them to form four bifurcated intercomponent hydrogen bonds without requiring any distortion in the conjugation of the isophthalamide systems (the amides are close to planar with the aromatic rings) while the macrocycle adopts a favorable chair conformation. The two hydrogen bond donor groups of the thread are satisfied in the solid state by included molecules of DMF, which pack to form additional π-stacks between the phenyl groups of the stoppers and the isophthaloyl rings of the macrocycle. A further characteristic of the system is the lack of sterically demanding sp^3 centers between the two hydrogen bond accepting groups on the thread, previously found[4b,d] to disrupt the complementarity between the flat, close fitting internal surfaces of the mechanically interlocked architecture. Indeed, the proportions of the thread serve to maximize attractive van der Waals interactions between the two components, with the olefin providing an additional π-stacking feature for the xylylene units of the macrocycle.

The success of the fumaramide template can thus be attributed to (i) the spatial arrangement of the cooperative hydrogen bonding sites on the thread which is close-to-ideal as a template for benzylic amide macrocycle formation, i.e., allows a low-energy (chair-type) conformation of the macrocycle precursor **3** to bind efficiently to the hydrogen bonding sites of the thread in the key supramolecular intermediate **II** (Scheme 2), (ii) the rigidity and shape of the template unit (no internal degrees of freedom of the thread are lost upon complexation with **3** to form **II**), and (iii) the inability of the free fumaramide thread **5** to fold and form intramolecular hydrogen bonds.

The use of amide groups in the thread is also significant, of course, because they are excellent hydrogen bond acceptors (H-bond basicity, β_2^H, typically ~0.66).[8] Indeed, among common functional group types, the β_2^H of amides is only exceeded by groups with pronounced mesomeric or ionic character (N^+-O^-, S^+-O^-, P^+-O^-, etc). However, preorganizing the hydrogen bonding sites of the thread into the ideal geometry illustrated in Figure 1 is *so* effective at enhancing the macrocyclic template effect that esters—significantly weaker hydrogen bond acceptors than amides ($\beta_2^H \sim 0.45$, similar to that of ethers and nitriles)—can also promote the cyclization of **3** to give mechanically interlocked architectures.

The threads **7** and **8**, replacing one and both secondary amides with ester groups respectively, both act as templates for benzylic amide macrocycle formation (Scheme 2), manifested in the formation of [2]rotaxanes **9** and **10** in yields of 35 and 3%, respectively.

While at first sight the yield of the bis-ester rotaxane **10** may appear modest at 3%, that the reaction proceeds at all is remarkable. Rotaxane formation is an entropically unfavorable five-component assembly process, occurring in direct competition with processes such as [2]catenane assembly which is promoted by the formation of up to six amide−amide hydrogen bonds.[9] The reaction takes place in the presence of high concentrations of amines, amides, and halide ions (the latter in the form of $Et_3N^+HCl^-$), all significantly stronger alternative hydrogen bond acceptors to esters, yet the yield of **10** is only 1 order of magnitude less than that obtained using the original bis-amide isophthalamide thread (28%).[4a] The crucial role played by the second binding site, and thus the full significance of preorganizing the cooperative binding sites in the thread, is evident from the comparative binding constants of di(*p*-butylphenyl)isophthalamide with Cl^- ion ($[PPh_4]^+Cl^-$: $K_a(CD_2Cl_2) = 6.1 \times 10^4\ M^{-1}$)[10] and a single, isolated ester group ($PhCO_2Me$: $K_a(CD_2Cl_2) < 10\ M^{-1}$)!

Gaining an understanding of amide−ester hydrogen bonding is of interest for areas as diverse as the design of peptide mimetics,[11a] D-Ala-D-Lac-binding "super bug" antibiotics,[11b] and the prediction of the structure and folding of commercially important synthetic polyamide/ester polymers.[11c] However, because of the many alternative more energetically favorable ways of satisfying amide hydrogen bonding requirements, amide−ester hydrogen bonds in the solid state are so rare that a recent[12] search found only 16 examples in the Cambridge Crystallographic Database. Together, the three isostructural rotaxanes **6**, **9**, and **10** thus provide an unprecedented model series with which to study the nature of amide−ester hydrogen bonding interactions, both in solution and the solid state.

The X-ray crystal structures of **9** and **10** are shown in Figure 2. Although the conformations of the central regions of the threads in all three rotaxane crystal structures are virtually superimposable, in the mono-ester (**9**) and bis-ester (**10**) rotaxanes the macrocycle is distorted from a chair conformation, and the conjugation of the isophthalamide units disrupted, to increase the number of amide−amide hydrogen bonds at the expense of weaker amide−ester hydrogen bonds. In the case of the mono-ester rotaxane, **9**, each macrocycle acts as a donor for three amide−amide hydrogen bonds (including a remarkable intermolecular bifurcated system, e.g. N11′H−O21−HN39′,

(8) Abraham, M. H. *Chem. Soc. Rev.* **1993**, *22*, 73−83.

(9) Johnston, A. G.; Leigh, D. A.; Pritchard, R. J.; Deegan, M. D. *Angew. Chem., Int. Ed. Engl.* **1995**, *34*, 1209−1212.

(10) Kavallieratos, K.; de Gala, S. R.; Austin, D. J.; Crabtree, R. H. *J. Am. Chem. Soc.* **1997**, *119*, 2325−2326.

(11) (a) *Peptide-based Drug Design*; Taylor, M. D., Amidon, G. L., Eds.; ACS: Washington, DC, 1995. (b) Williams, D. H.; Bardsley, B. *Angew. Chem., Int. Ed. Engl.* **1999**, *38*, 1172−1193. (c) *Macromolecular Design of Polymeric Materials*; Hatada, K., Kitayama, T., Vogl, O., Eds.; Marcel Dekker: New York, 1997.

(12) Alemán, C.; Navas, J. J.; Muñoz-Guerra, S. *J. Phys. Chem.* **1995**, *99*, 17653−17661.

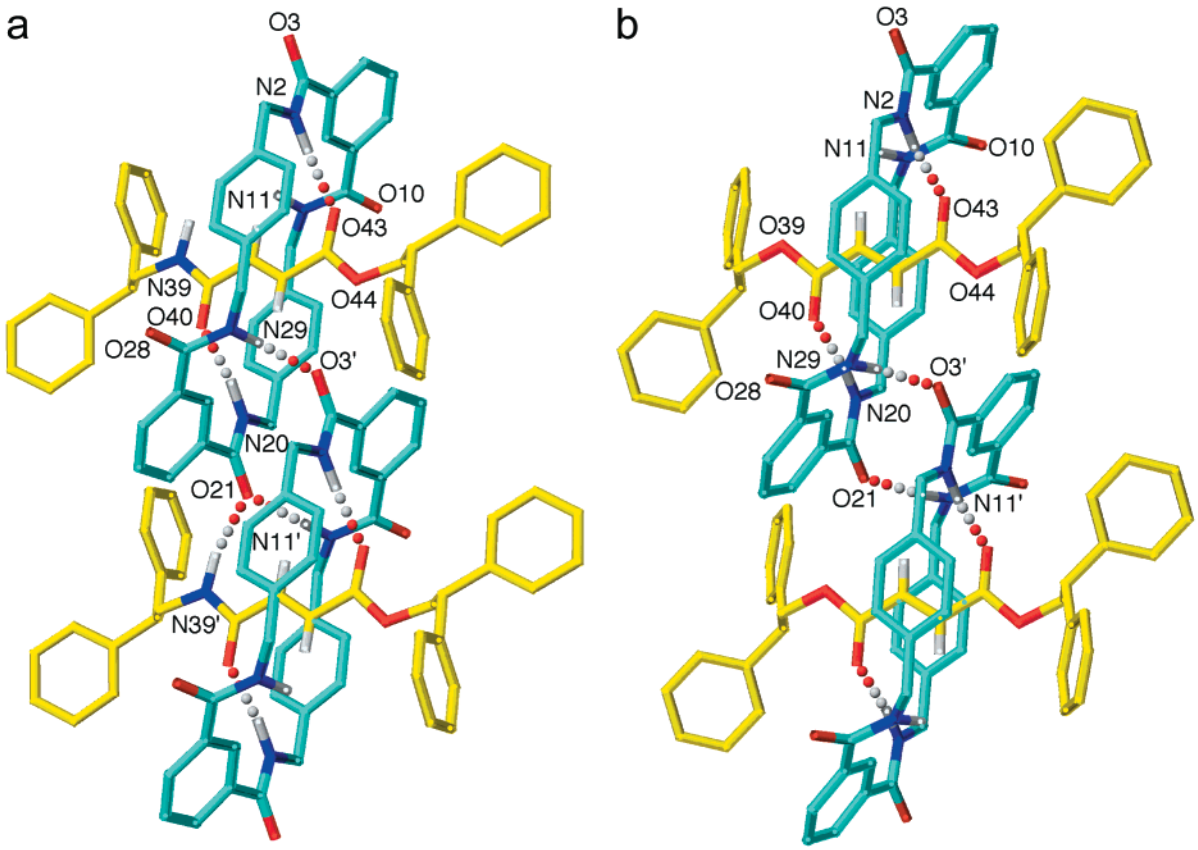

Figure 2. X-ray crystal structure of (a) the mixed amide-ester [2]rotaxane **9** and (b) the bis-ester [2]rotaxane **10**. Intramolecular hydrogen bond distances (Å) are the following: (a) O43−HN2 1.90, O40−HN20 1.87; (b) O43−HN11/O40−HN20 1.88. Intermolecular hydrogen bond distances (Å) are the following: (a) O3′−HN29/O21−HN11′ 2.01, O21−HN39′ 2.05; (b) O3′−HN29/O21−HN11′ 1.93.

Figure 2a) and a single amide−ester one (O43−HN2), with the thread amide also acting as a donor for a further amide−amide hydrogen bond (O21−HN39′). In the bis-ester rotaxane, **10**, the macrocycle acts as the donor for two amide−amide and two amide−ester hydrogen bonds. In both **9** and **10**, only two of the hydrogen bonds are formed via intramolecular, intercomponent interactions in the solid state compared to the maximum number possible (four) seen for the fumaramide rotaxane **6**.

To show that the differences between the fumaramide rotaxane **6** and the ester-containing systems, **9** and **10**, were not a consequence of the number of hydrogen bond donors present in the thread, the bis-tertiary amide thread **11** was prepared. As with the bis-secondary amide thread, **5**, rotaxane formation proceeds in high yield (67%) to give **12** and the solid-state structure of crystals grown from acetonitrile (Figure 3) shows the double bifurcated hydrogen bond motif between the two rotaxane components.

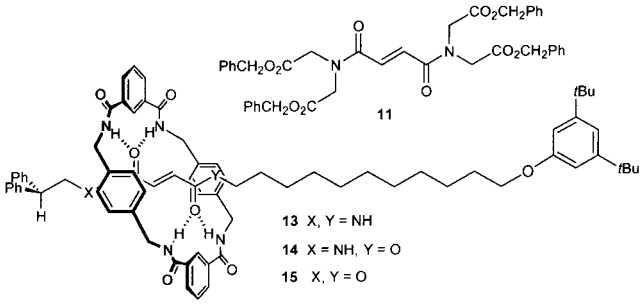

In solution the individual rotaxane molecules are isolated from each other and the components *must* adopt intramolecular hydrogen bonding patterns to lower their energy, the most stable

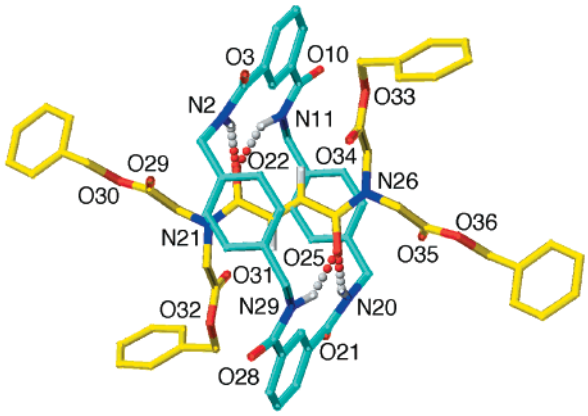

Figure 3. X-ray crystal structure of the tertiary amide fumaramide [2]rotaxane **12**. Intramolecular hydrogen bond distances (Å) are the following: O22−HN2/O25−HN20 2.16, O22−HN11/O25−HN29 2.40.

structure for each rotaxane presumably involving two sets of bifurcated hydrogen bonds analogous to the solid-state structures of **6** and **12**. The ^{1}H NMR spectra ($CDCl_3$, 400 MHz, 298 K) of the isostructural threads and rotaxanes which differ only in the number of amide and ester hydrogen bond acceptors (i.e. **5**−**10**, Figure 4) gives information regarding the intercomponent hydrogen bonding in the rotaxanes in solution (and an indication of the strength of hydrogen bonding in the supramolecular intermediate **II** responsible for the template effect).

Comparison of the spectra in Figure 4 shows that the predominant co-conformations adopted in solution by the mechanically interlocked components are, indeed, similar for all three rotaxanes, hydrogen bonding locating the macrocycle over the olefin, as indicated by the virtually identical shift-

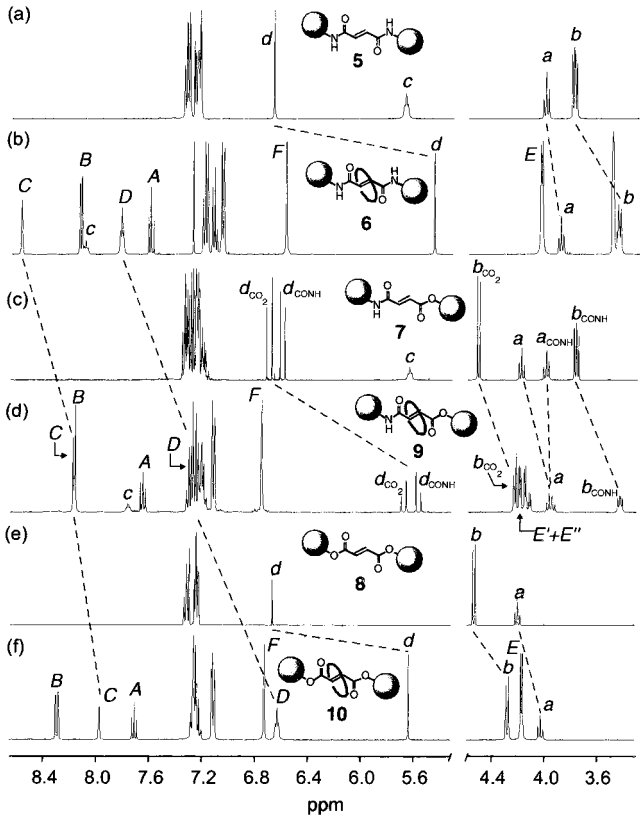

Figure 4. ^{1}H NMR spectra (400 MHz, $CDCl_3$, 298K) of (a) **5**, (b) **6**, (c) **7**, (d) **9**, (e) **8**, and (f) **10**.

differences between thread and rotaxane in each case for the olefin (H_d) and stopper protons (H_a and H_b). The *strength* of the hydrogen bonding between the components in each case, however, is very different. Initially, this is suggested by the relative chemical shifts of the macrocycle amide protons (H_D) in **6** (δ 7.83), **9** (δ 7.15), and **10** (δ 6.66), the downfield position being an indication of the degree of their involvement in hydrogen bonding, although this is not a clear-cut measurement since amide and ester carbonyl groups have different bond anisotropies and electric field strengths. However, the H_C protons of the macrocycle, which are held in the shielding region of a carbonyl group during bifurcated hydrogen bonding, follow a similarly consistent pattern of behavior, being shielded to a much greater degree in **6** than in **9** or **10**.

Variable-temperature (VT) ^{1}H NMR experiments provide a definitive measure of the relative strengths of the intercomponent hydrogen bonding through the respective energy barriers to pirouetting of the macrocycle about the threads. A combination of NMR methods[13,14] (because of the different time regimes involved) were carried out on **12** and (for reasons of solubility) **13**−**15**, alkyl chain derivatives of **6**, **9**, and **10**, to give barriers of rotation at 298 K in CD_2Cl_2 of **12** ($\Delta G = 13.4 \pm 0.1$ kcal mol^{-1}; SPT-SIR), **13** ($\Delta G = 11.5 \pm 0.2$ kcal mol^{-1}; coalescence), **14** ($\Delta G = 9.3 \pm 0.2$ kcal mol^{-1}; coalescence), and **15** ($\Delta G = 7.2 \pm 0.4$ kcal mol^{-1}; estimated value based upon line broadening). Assuming the mechanism of ring rotation is the same in each case, the differences in energy barriers of 2.2 kcal mol^{-1} between the fumaramide rotaxane **13** and the monoamide−monoester **14** and the 2.1 kcal mol^{-1} difference between

(13) Dahlquist, F. W.; Longmur, K. J.; Du Vernet, R. B. *J. Magn. Reson.* **1975**, *17*, 406. For applications of SPT-SIR to dynamic processes in rotaxanes see ref 4d.

(14) Sandström, J. *Dynamic NMR Spectroscopy*; Academic Press: London, 1982.

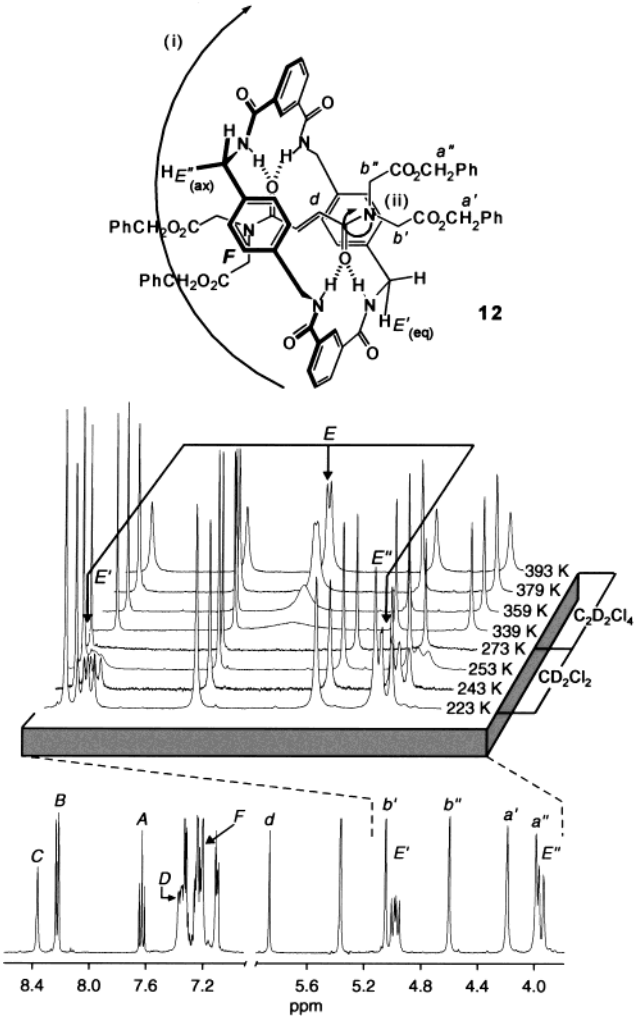

Figure 5. Dynamic processes in a [2]rotaxane. ^{1}H NMR spectrum (400 MHz) of **12** in CD_2Cl_2 at 223 K (main trace), showing (i) slow pirouetting of the macrocycle about the thread ($H_{E'}$ and $H_{E''}$ resolved) and (ii) slow rotation of the tertiary amide N−C bond ($H_{a'}$ and $H_{a''}$/$H_{b'}$ and $H_{b''}$ resolved). SPT-SIR between resolved signals gives energy barriers for tertiary amide rotation (20.4 ± 0.1 kcal mol^{-1}) and macrocycle pirouetting (13.4 ± 0.1 kcal mol^{-1}). Higher temperature spectra (expansion, 223−273 K (CD_2Cl_2) and 339−393 K ($C_2D_2Cl_4$)) illustrate the wide temperature ranges (170° for $H_{E'}$/$H_{E''}$ → H_E!) that can exist between full resolution and coalescence of signals affected by dynamic processes in mechanically interlocked molecules.

14 and the bis-ester rotaxane **15** can largely be attributed to the difference in hydrogen bond strength between two −NH bifurcated hydrogen bonds to an amide rather than an ester, i.e., under these conditions a −NH···O═CNH− hydrogen bond is just over 1 kcal mol^{-1} stronger than the analogous −NH···O═CO− interaction.

^{1}H NMR spectroscopy also provides a window through which to observe the remarkable sequence of intra- and intercomponent dynamic processes present in a simple amide-based rotaxane, including (i) macrocycle pirouetting and (ii) amide bond rotamerization, illustrated through the VT ^{1}H NMR spectra of **12** in CD_2Cl_2 (low temperature) and $C_2D_2Cl_4$ (high temperature) given in Figure 5. Spin polarization transfer by selective inversion recovery (SPT-SIR)[13] on $H_{a'}$ to $H_{a''}$ and $H_{b'}$ to $H_{b''}$ shows that tertiary amide rotamerization in the rotaxane has a significantly higher energy barrier (20.4 ± 0.1 kcal mol^{-1}) than a conventional tertiary amide (∼18.4 kcal mol^{-1}), attributable to intercomponent hydrogen bonding stabilizing the R_2N^+═C−O^- resonance contribution of the tertiary amide group.[4d]

Furthermore, a combination of NMR spectroscopy, Kerr-effect measurements, and molecular modeling recently uncovered a remarkable new property of component dynamics in these mechanically interlocked architectures; the rate of macrocycle pirouetting in rotaxanes such as **6** can be varied through the use of an oscillating electric field.[15] This offers a potentially extremely useful method for controlling rotaxane movements in molecular-based devices.

Conclusions

Fixing multiple cooperative binding sites in an ideal spatial arrangement on a structurally rigid backbone is a powerful method for facilitating the hydrogen bond-directed synthesis of rotaxanes, with the fumaramide motif providing one of the most accessible and efficient rotaxane syntheses described to date. Preorganizing the template is so effective that modest hydrogen bonding groups can be used to template multicomponent assembly processes, *even in the presence of far more potent, but not preorganized, hydrogen bonding groups!* It is interesting to note that cooperative interactions, organization, and structural rigidity are key elements in the mode of action of LY333328, the "super-bug" antibiotic that binds weakly to the ester-terminated D-Ala-D-Lac sequence on the cell surfaces of vancomycin-resistant enterococci.[11b]

Experimental Section

General Method for the Preparation of Benzylic Amide Macrocycle Fumaryl-Based [2]Rotaxanes. The threads **5**, **7**, **8**, or **11** (1.00 mmol) and triethylamine (2.1 mL, 15.7 mmol) were dissolved in 100 mL of chloroform (stabilized with amylenes) or, in the case of **5**, 1:9 acetonitrile:chloroform and the mixtures were stirred vigorously while solutions of the diamine (1.09 g, 4 equiv) in chloroform (45 mL) and the acid chloride (1.62 g, 4 equiv) in chloroform (45 mL) were simultaneously added over a period of 2 h using motor-driven syringe pumps. After a further 2 h the resulting suspension was filtered and concentrated under reduced pressure to leave, in general, only the unconsumed thread and [2]rotaxane. This mixture was subjected to column chromatography (silica gel, CH_2Cl_2/MeOH as eluent) to yield, in order of elution, the unconsumed thread and the [2]rotaxane. In the case of **6**, the rotaxane was obtained directly from the concentrated reaction filtrate by spontaneous crystallization promoted by the addition of water to a solution of the crude product in dimethylformamide (30 mL). Selected data for [2]-(1,7,14,20-tetraaza-2,6,15,19-tetraoxo-3,5,9,12,16,18,22,25-tetrabenzocyclohexacosane)-(*E*)-(*N*,*N*′-bis(2′,2′-diphenylethyl)-2′-butendiamide)rotaxane (**6**): yield 0.97 g (97%); mp 355−356 °C (DMF/H_2O); ^{1}H NMR (400 MHz, DMSO-d_6) δ 3.67 (dd, J = 7.9, 5.9 Hz, 4H, CHCH_2NH), 4.11 (t, J = 7.9 Hz, 2H, CH), 4.22 (d, J = 5.0 Hz, 8H, H_E), 5.66 (s, 2H, CH═), 6.66 (s, 8H, ArH_F), 7.12−7.35 (m, 20H, ArH), 7.73 (t, J = 7.8 Hz, 2H, ArH_A), 8.01 (dd, J = 7.8, 1.4 Hz, 4H, ArH_B), 8.15 (t, J = 5.0 Hz, 4H, NH_D), 8.53 (t, J = 5.9 Hz, 2H, NH), and 8.63 (s, b, 2H, ArH_C); ^{13}C NMR (100 MHz, DMSO-d_6) δ 43.6, 44.0, 50.3, 125.7, 126.9, 128.1, 128.77, 128.89, 129.45, 129.6, 131.1, 134.6, 136.7, 143.0, 165.7, 166.1; MS (FAB, mNBA) m/z 1029 [(rotaxane + Na)$^+$]. Anal. Calcd for $C_{64}H_{58}N_6O_6$: C 76.32, H 5.80, N 8.34. Found: C 76.42, H 5.71, N 8.29. Selected data for [2]-(1,7,14,20-tetraaza-2,6,15,19-tetraoxo-3,5,9,12,16,18,22,25-tetrabenzocyclohexacosane)-2,2-diphenyl-(*E*)-4-[(2,2-diphenylethyl)amino]-4-oxo-2-butenoate)rotaxane (**8**): yield 0.35 g (35%); mp 246−247 °C; ^{1}H NMR (400 MHz, $CDCl_3$) δ 3.67 (dd, J = 7.8, 5.8 Hz, 2H, CH_2-NH), 4.18 (t, J = 7.9 Hz, 1H, C*H*CH_2NH), 4.20 (t, J = 7.5 Hz, 1H, C*H*CH_2O), 4.37 (AB system, J = 14.3, 5.0 Hz, 8H, $H_{E'/E''}$), 4.46 (d, J = 7.5 Hz, CHCH_2O), 5.59 (d, J = 15.3 Hz, 1H, C*H*═CHCOO), 5.71 (d, J = 15.3 Hz, 1H, CH═C*H*COO), 6.67 (s, 8H, ArH_F), 7.10−7.36 (m, 21H, ArH + NH_D), 7.66 (t, J = 8.1 Hz, 2H, ArH_A), 7.78 (t, J = 5.9 Hz, 1H, NH), 8.18 (m, 6H, ArH_B + ArH_C); ^{13}C NMR (100 MHz, $CDCl_3$) δ 44.27, 44.40, 45.28, 49.77, 50.44, 68.84, 124.61, 127.15, 127.63, 128.17, 128.30, 129.13, 129.15, 129.55, 129.80, 131.75, 134.41, 134.97, 137.44, 140.73, 142.00, 164.90, 167.22, 167.34; MS (FAB, mNBA) m/z 1008 [(rotaxane + H)$^+$]. Anal. Calcd for $C_{64}H_{57}N_5O_7$: C 76.25, H 5.82, N 6.95. Found: C 76.37, H 5.82, N 6.85. Selected data for [2]-(1,7,14,20-tetraaza-2,6,15,19-tetraoxo-3,5,9,12,16,18,22,25-tetrabenzocyclohexacosane)bis(2,2-diphenylethyl)-(*E*)-2-butenedioate)-rotaxane (**10**): yield 0.03 g (3%); ^{1}H NMR (400 MHz, $CDCl_3$) δ 4.26 (t, J = 7.8 Hz, 2H, CH), 4.41 (d, J = 5.3 Hz, 8H, H_E), 4.51 (d, J = 7.8 Hz, 4H, CHCH_2O), 5.67 (s, 2H, CH═), 6.66 (t, J = 5.1 Hz, 4H, NH_D), 6.76 (s, 8H, ArH_F), 7.15 (d, J = 8.3 Hz, 8H, ArH), 7.23−7.32 (m, 12H, ArH), 7.74 (t, J = 7.8 Hz, 2H, ArH_A), 8.01 (s, 2H, ArH_C), 8.32 (d, J = 7.8 Hz, 4H, ArH_B); ^{13}C NMR (100 MHz, $CDCl_3$) δ 44.21, 49.85, 66.25, 122.65, 122.72, 127.87. 128.25, 129.35 129.40, 130.25, 131.18, 132.41, 134.45, 137.73, 140.41, 166.46; MS (FAB, mNBA) m/z 1009 [(rotaxane + H)$^+$]. Selected data for [2](1,7,14,20-tetraaza-2,6,15,19-tetraoxo-3,5,9,12,16,18,22,25-tetrabenzocyclohexacosane)benzyl-2-([[2-(benzyloxy)-2-oxoethyl]((*E*)-5-(bis[2-(benzyloxy)-2-oxoethyl]-amino))2,5-dioxo-3-pentenylamino]acetate)rotaxane (**12**): yield 0.83 g (67%); mp 268−269 °C; ^{1}H NMR ($CDCl_3$, 400 MHz) δ 3.91 (s, 4H, $H_{a'}$), 3.90 (bs, $H_{E'}$), 4.16 (s, 4H, $H_{a''}$), 4.66 (s, 4H, $H_{b'}$), 4.95 (bs, $H_{E''}$), 5.12 (s, 4H, $H_{b''}$), 5.92 (s, 2H, H_d), 7.11−7.42 (m, 32H, ArH + NH_D + ArH_F), 7.58 (t, J = 7.8 Hz, 2H, ArH_A), 8.30 (dd, J = 1.5, 7.8 Hz, 4H, ArH_B), 8.39 (bs, 2H, ArH_C); ^{13}C NMR (100 MHz, $CDCl_3$) δ 49.57, 50.23, 67.94, 68.09, 122.39, 128.58−129.92, 132.46, 134.36, 134.74, 132.46, 138.27, 166.0, 168.63, 166.71, 67.73, 168.27; LSIMS, m/z 1239 [(rotaxane + H)$^+$], 1262 [(rotaxane + Na)$^+$]. Anal. Calcd for $C_{72}H_{66}N_6O_{14}$: C 69.78, H 5.37, N 6.78. Found: C 69.46, H 5.33, N.6.58.

X-ray Crystallographic Structure Determinations. 6: $C_{68}H_{56}N_6O_6$, M = 1007.16, crystal size 0.01 × 0.03 × 0.05 mm, triclinic $P\bar{1}$, a = 15.1820(2) Å, b = 21.2255(2) Å, c = 21.5668(3) Å, α = 65.8240(10)°, β = 83.8570(10)°, γ = 78.1380(10)°, V = 6202.83(13) Å^3, Z = 4, ρ_{calcd} = 1.235 Mg m^{-3}; synchrotron radiation (CLRC Daresbury Laboratory Station 9.8, silicon monochromator, λ = 0.6883 Å), μ = 0.082 mm^{-1}, T = 150(2) K. 36861 data (22685 unique, R_{int} = 0.1774, 1.00 < θ < 27.18°) were collected on a Siemens SMART CCD diffractometer using narrow frames (0.3° in ω) and were corrected semiempirically for absorption and incident beam decay (transmission 0.58−1.00). The structure was solved by direct methods and refined by full-matrix least-squares on F^2 values of all data (G. M. Sheldrick, SHELXTL manual, Siemens Analytical X-ray Instruments, Madison WI, 1994, version 5) to give $wR = \{\sum[w(F_o^2 - F_c^2)^2]/\sum[w(F_o^2)^2]\}^{1/2}$ = 0.5259, conventional R = 0.3240 for F values of 22635 reflections with $F_o^2 > 2\sigma(F_o^2)$, S = 1.156 for 850 parameters. Residual electron density extremes were 0.527 and −0.413 Å^{-3}. Due to the scarcity of observed data, all the oxygen and nitrogen atoms were refined anisotropically while all the carbon atoms were refined isotropically. Amide hydrogen atoms were refined isotropically subject to a distance constraint N−H = 0.98 Å, with the remainder constrained. Despite the rather high R factor and wR value due to disorder in the DMF molecules, the results permit an unambiguous determination of connectivity, packing pattern, the spatial relationship between macrocycle, thread, and solvent, their conformations, and the intercomponent hydrogen bonding motifs.

Experimental details for **9**, **10**, and **12** were the same as for **6** except for the following: **9:** $C_{64}H_{57}N_5O_7$, M = 1008.15, crystal size 0.06 × 0.14 × 0.14 mm, monoclinic Cc, a = 11.6650(5)Å, b = 15.6465(8) Å, c = 28.4397(13) Å, β = 96.653(2)°, V = 5155.8(8) Å^3, Z = 4, ρ_{calcd} = 1.299 g cm^{-3}; Mo $K\alpha$ radiation (graphite monochromator, λ = 0.71073 Å), μ = 0.085 mm^{-1}, T = 298(2) K. 11030 data (6202 unique, R_{int} = 0.0726, 2.19 < θ < 23.26°) were collected on a Siemens SMART CCD diffractometer using narrow frames (0.3° in ω) and were corrected semiempirically for absorption and crystal decay (transmission 0.31−1.00). The structure was solved and refined as described above for **6** to give $wR = \{\sum[w(F_o^2 - F_c^2)^2]/\sum[w(F_o^2)^2]\}^{1/2}$ = 0.1966, conventional R = 0.0667 for F values of 6202 reflections with $F_o^2 > 2\sigma(F_o^2)$, S = 0.934 for 705 parameters. Residual electron density extremes were 0.160 and −0.204 Å^{-3}. Amide hydrogen atoms were refined isotropically subject to a distance constraint N−H = 0.98 Å, with the remainder constrained; anisotropic displacement parameters were used for all non-hydrogen atoms. **10:** $C_{64}H_{56}N_4O_8$, M = 1009.13,

(15) Bermudez, V.; Capron, N.; Gase, T.; Gatti, F. G.; Kajzar, F.; Leigh, D. A.; Zerbetto, F.; Zhang, S. *Nature* **2000**, *406*, 608−611.

crystal size 0.04 × 0.13 × 0.2 mm, triclinic $P\bar{1}$, $a = 9.7839(7)$ Å, $b = 10.9115(7)$ Å, $c = 15.0045(10)$ Å, $\alpha = 82.5130(10)°$, $\beta = 87.3340(10)°$, $\gamma = 77.8280(10)°$, $V = 1552.2(2)$ Å^3, $Z = 1$, $\rho_{calcd} = 1.335$ g cm^{-3}; Mo $K\alpha$ radiation (graphite monochromator, $\lambda = 0.71073$ Å), $\mu = 0.335$ mm^{-1}, $T = 298(2)$ K. 9819 data (4454 unique, $R_{int} = 0.0321$, $1.92 < \theta < 23.29°$) were collected on a Siemens SMART CCD diffractometer using narrow frames (0.3° in ω) and were corrected semiempirically for absorption and incident beam decay (transmission 0.71−1.00). The structure was solved and refined as described above for **6** to give $wR = \{\sum[w(F_o^2 - F_c^2)^2]/\sum[w(F_o^2)^2]\}^{1/2} = 0.1231$, conventional $R = 0.0442$ for F values of 4454 reflections with $F_o^2 > 2\sigma(F_o^2)$, $S = 0.930$ for 388 parameters. Residual electron density extremes were 0.321 and −0.277 Å^{-3}. Amide hydrogen atoms were refined isotropically subject to a distance constraint of N−H = 0.98 Å, with the remainder constrained; anisotropic displacement parameters were used for all non-hydrogen atoms. **12:** $C_{72}H_{66}N_6O_{14}$, $M = 1239.31$, crystal size 0.12 × 0.13 × 0.24 mm, rhombohedral $R\bar{3}$, $a = 41.875(2)$ Å, $b = 41.875(2)$ Å, $c = 10.6871(9)$ Å, $\alpha = 90°$, $\beta = 90°$, $\gamma = 120°$, $V = 16229.4(19)$ Å^3, $Z = 9$, $\rho_{calcd} = 1.141$ g cm^{-3}; Mo $K\alpha$ radiation (graphite monochromator, $\lambda = 0.71073$ Å), $\mu = 0.080$ mm^{-1}, $T = 293(2)$ K. 23900 data (5187 unique, $R_{int} = 0.0900$, $1.68 < \theta < 23.26°$) were collected on a Siemens SMART CCD diffractometer using narrow frames (0.3° in ω) and were corrected semiempirically for absorption and incident beam decay (transmission 0.15−1.00). The structure was solved and refined as described above for **6** to give $wR = \{\sum[w(F_o^2 - F_c^2)^2]/\sum[w(F_o^2)^2]\}^{1/2} = 0.3492$, conventional $R = 0.0984$ for F values of 5187 reflections with $F_o^2 > 2\sigma(F_o^2)$, $S = 0.805$ for 412 parameters. Residual electron density extremes were 0.383 and −0.311 Å^{-3}. Amide hydrogen atoms were refined isotropically subject to a distance constraint of N−H = 0.98 Å, with the remainder constrained; anisotropic displacement parameters were used for all non-hydrogen atoms.

Crystallographic data for **6**, **9**, **10**, and **12** (excluding structure factors) have been deposited with the Cambridge Crystallographic Data Centre as supplementary publication numbers CCDC-140045 (**6**), CCDC-140046 (**9**), CCDC-140047 (**10**), and CCDC-140048 (**12**). Copies of the data can be obtained free of charge on application to The Director, CCDC, 12 Union Road, Cambridge CB2 1EZ, UK (fax Int. code + (1223)336-033; e-mail teched@chemcrys.cam.ac.uk).

Acknowledgment. This work was supported through the EU TMR Network contract FMRX-CT96-0059 and the EPSRC. F.G.G. and D.A.L. are Marie Curie (FMBI-CT97-2834) and EPSRC Advanced (AF/982324) Research Fellows, respectively. We thank G. Priimov (University of Warwick) for providing samples of **13**−**15**.

Supporting Information Available: Tables of crystal data, structure solution and refinement, atomic coordinates, bond lengths and angles, and anisotropic thermal parameters for **6**, **9**, **10**, and **12** (PDF). This material is available free of charge via the Internet at http://pubs.acs.org. The atomic coordinates for this structure have been deposited with the Cambridge Crystallographic Data Centre. The coordinates can be obtained, on request, from the Director, Cambridge Crystallographic Data Centre, 12 Union Road, Cambridge, CB2 1EZ, UK.

JA001697R